NJC

# Tetraphenylethene–anthracene-based fluorescence emission sensor for detection of water with photo-induced electron transfer and aggregation-induced emission characteristics

| | |
|---|---|
| Journal: | *New Journal of Chemistry* |
| Manuscript ID | NJ-ART-04-2022-001599.R1 |
| Article Type: | Paper |
| Date Submitted by the Author: | 27-Apr-2022 |
| Complete List of Authors: | Nishimoto, Emiko; Hiroshima University<br>Mise, Yuta; Hiroshima University,<br>Fumoto, Takuma; Hiroshima University<br>Miho, Saori; Hiroshima University<br>Tsunoji, Nao; Hiroshima University,<br>Imato, Keiichi; Hiroshima University, Department of Applied Chemistry<br>Ooyama, Yousuke; Hiroshima University, |
| | |

ARTICLE

# Tetraphenylethene–anthracene-based fluorescence emission sensor for detection of water with photo-induced electron transfer and aggregation-induced emission characteristics

Received 00th January 20xx,
Accepted 00th January 20xx

DOI: 10.1039/x0xx00000x

Emiko Nishimoto, Yuta Mise, Takuma Fumoto, Saori Miho, Nao Tsunoji, Keiichi Imato and Yousuke Ooyama*

As a fluorescent sensor for water over a wide range from low to high water content regions in organic solvents, we have designed and developed a PET (photo-induced electron transfer)/AIE (aggregation-induced emission)-based fluorescent sensor **EN-1** composed of a tetraphenylethene (TPE) core and four anthracene-(aminomethyl)-4-cyanophenylboronic acid pinacol esters (AminoMeCNPhenylBPin) as peripheral units. **EN-1** showed an enhancement of the fluorescence band at around 450 nm originating from the anthracene skeleton with increasing the water content in THF in the low water content region below 1.0 wt%, which is attributed to the formation of PET inactive (fluorescent) species **EN-1($H_2O$)** by the addition of water molecules. With increasing the water content from 10 wt% to 50 wt%, the fluorescence intensity at around 500 nm originating from the TPE core gradually increased, which is attributed to the restricted intramolecular rotation (RIR) of TPE due to the increase in viscosity of the THF-water mixtures. Furthermore, a significant enhancement of the fluorescence band at around 470 nm in the water content region above 60 wt% was observed due to the AIE characteristics associated with aggregate formation of **EN-1($H_2O$)-A** in both PET inactive and RIR states. The detection limit (DL) of **EN-1** for water in the low water content region below 1.0 wt% in THF was 0.21 wt%, which is superior to that (DL = 0.49 wt%) of **RS-1** composed of a TPE unit and an anthracene-AminoMeCNPhenylBPin unit. Moreover, the AIE characteristics of **EN-1** were observed from the relatively low water content of 60 wt% compared with those of **RS-1**, which were observed in the high water content region over 75 wt%. The improvement of the DL value and AIE characteristics of **EN-1** is ascribable to the fact that the four anthracene-AminoMeCNPhenylBPin units led to the increased fluorescence emission originating from the anthracene skeleton and its low solubility in solvent-water mixtures, compared with **RS-1**. Consequently, this work reveals that **EN-1** composed of a TPE core and four anthracene-AminoMeCNPhenylBPin units can act as a PET/AIE-based fluorescent sensor for detection of water in a low water content region and from moderate to high water content regions in solvents.

## Introduction

Development of fluorescent sensors for water is of growing significance to construction of a highly sensitive and quick flow fluorescence spectral analysis for detection and quantification of water over a wide range from low to high water content in solutions, solids, gasses, and the products, based on changes in wavelength, intensity, and lifetime of fluorescence emission depending on the water content.[1–11] Moreover, fluorescent sensors for water have the potential to be functional materials, which allow visualization as well as detection and quantification of moisture or water droplets on material surfaces, and promise to be applied to environmental, biomedical, and quality control monitoring systems.[12–18] Indeed, various kinds of organic fluorescent sensors for the determination of water content in solvents based on their intramolecular charge transfer (ICT),[19–29] excited state intramolecular proton transfer (ESIPT),[30–33] photo-induced electron transfer (PET)[34–41] or solvatofluorochromic properties[42–47] have been designed and developed. The effects of ICT, PET, and ESIPT on the fluorescent sensing properties for the detection of water were investigated based on the intermolecular interactions of the fluorescent sensors with water molecules, which demonstrated that ICT-, PET-, and ESIPT-based fluorescent sensors were suitable for the detection and quantification of a trace amount of water (below 1–10 wt% in almost every case) in solvents. In fact, the detection limits (DLs) of these fluorescent sensors were as low as 0.01–0.001 wt% for water in solvents. However, the ICT- and ESIPT-based fluorescent sensors showed attenuation of the fluorescence emission with the increase in water content in solvents, that is, fluorescence quenching (turn-off) systems that made it difficult to visually confirm the presence of water in samples and on material surfaces. In contrast, the PET-based fluorescent sensors showed enhancement of the fluorescence emission with the increase in water content in solvents, that is, a fluorescence enhancement (turn-on) system that made it possible to visually confirm the presence of water in samples and on material surfaces by reversible changes in the immediate environment due

*Applied Chemistry Program, Graduate School of Advanced Science and Engineering, Hiroshima University, 1-4-1 Kagamiyama, Higashi-Hiroshima 739-8527, Japan. E-mail: yooyama@hiroshima-u.ac.jp*
Electronic Supplementary Information (ESI) available: See DOI: 10.1039/x0xx00000x

to the reversible intermolecular interactions between the sensors and water molecules. We have designed and developed anthracene-(aminomethyl)-4-cyanophenylboronic acid pinacol ester (AminoMeCNPhenylBPin) **OF-2** as a PET-based fluorescent sensor for a trace amount of water (Fig. 1a).[37] In **OF-2**, the PET takes place from the nitrogen atom of the amino moiety to the photoexcited fluorophore (anthracene skeleton) in the absence of water, quenching the fluorescence. When water was added to the solution of **OF-2**, a drastic enhancement of the fluorescence emission was observed due to the suppression of PET, in which the nitrogen atom of the amino moiety was protonated or strongly interacted with water molecules, leading to the formation of the PET inactive (fluorescent) species **OF-2(H$_2$O)**. It was found that the DL values of **OF-2** for water were 0.01 wt% in 1,4-dioxane, 0.008 wt% in THF, 0.009 wt% in acetonitrile, and 0.009 wt% in ethanol, respectively, and equivalent or superior to those of the fluorescence quenching systems (turn-off) based on the ICT-[19–29] and ESIPT-based[30–33] fluorescent sensors. Furthermore, to develop fluorescent polymeric materials for visualization and detection of water, we have achieved the preparation of various types of polymer films (polystyrene, poly(4-vinylphenol), polyvinyl alcohol, and polyethylene glycol) doped with **OF-2**.[17] It was found that the **OF-2**-doped polymer films exhibited a reversible switching of the fluorescent color between the green excimer emission in the PET active state under a drying process and the blue monomer emission in the PET inactive state upon exposure to moisture or water droplets. Thus, we demonstrated that the fluorescence enhancement (turn-on) system of the PET-based fluorescent sensor was suitable for the visualization as well as detection and quantification of a trace amount of water in samples and on material surfaces. Meanwhile, as another fluorescence enhancement system for the detection of water, there is aggregation-induced emission (AIE) of organic fluorophores, that is, the emission enhancement induced by aggregate formation of the organic fluorophores usually upon addition of water into the solutions.[48–71] Tetraphenylethene (TPE), diphenyldibenzofulvene (DPDBF), and their derivatives are typical AIE-active fluorophores.[56–71] TPE- or DPDBF-based compounds in dilute solutions exhibited almost no emission due to the radiationless relaxation of the excitons by dynamic rotation of the phenyl groups. Upon aggregate formation by addition of large amounts of water (over 60 wt% in almost every case) into the solutions, on the other hand, the TPE- or DPDBF-based compounds exhibited AIE characteristics due to the restricted intramolecular rotation (RIR) of the phenyl groups, which eliminates the radiationless (non-emissive) relaxation of the photoexcited fluorophores. Tanaka et al. have reported fluorescent sensing properties of fluorophore-*o*-carborane dyads possessing unique AIE characteristics for the detection of water.[72–74] In contrast to PET-based fluorescent sensors, AIE-based fluorescent sensors are suitable for the detection of water in solvents containing high water content. Therefore, construction of a fluorescence enhancement (turn-on) method for the detection of water over a wide range from low to high water content regions in samples and on material surfaces is the grand challenge to achieve the practical use of fluorescent sensors for water in environmental and quality control monitoring systems and industry.

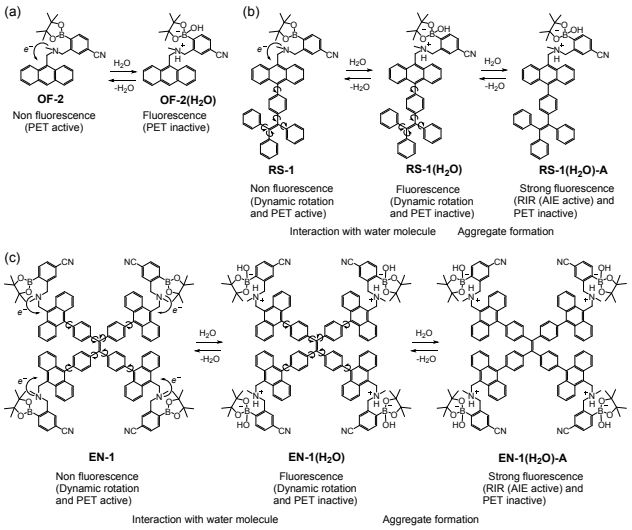


**Fig. 1** Mechanisms of fluorescent sensors: (a) PET-based sensor **OF-2** and PET/AIE-based sensors (b) **RS-1** (previous work) and (c) **EN-1** (this work) for detection of water in organic solvents.

For this purpose, in our previous work, we have designed and developed TPE–anthracene-AminoMeCNPhenylBPin **RS-1** possessing PET and AIE characteristics as a PET/AIE-based fluorescent sensor for the detection of water over a wide range from low to high water content in solvents, where the TPE unit is directly attached to the 10-position of the anthracene skeleton (Fig. 1b).[75] It was found that the enhancement of the fluorescence band at ca. 430 nm originating from the anthracene skeleton with increasing the water content in THF in the low water content region below 1.0 wt% was due to the formation of the PET inactive species **RS-1(H$_2$O)** by the addition of a water molecule. Subsequently, the AIE characteristics due to the RIR of the TPE unit associated with aggregate formation (**RS-1(H$_2$O)-A**) were observed as an enhanced fluorescence band at ca. 450 nm in the high water content region over 75 wt%. The main advantage of the PET/AIE-based fluorescent sensor is to make it possible to detect water in the low and high water content regions, compared to each PET-based and AIE-based fluorescent sensor alone, which is suitable for the detection of water in the low and high water content regions, respectively. However, one can see that the disadvantage of the PET/AIE-based fluorescent sensor is to give no response in the moderate and wide water content region from ca. 1.0 wt% to ca. 80 wt%, in which the fluorescence intensity does not increase linearly with the increase in the water content. In addition, the DL value of **RS-1** for water in the low water content region below 1.0 wt% in THF was 0.249 wt%, which was much inferior to that (DL = 0.008 wt%) of the PET-based fluorescent sensor **OF-2**.[37] Therefore, developing a more efficient PET/AIE-based fluorescent sensor is necessary to not only overcome the non-response range (the moderate and wide water content region) but also improve the DL for the detection of water in solvents.

Thus, in this work, as a fluorescent sensor for water over a wide range from low to high water content regions in organic solvents, we have designed and developed a PET/AIE-based fluorescent sensor **EN-1** composed of a TPE core and four anthracene-AminoMeCNPhenylBPin as peripheral units (Fig. 1c). The four anthracene-AminoMeCNPhenylBPin units are expected to improve the DL value and AIE characteristics of **EN-1** in a relatively low water content region due to the increased fluorescence emission originating from the anthracene skeleton and its low solubility in solvent-water mixtures, compared with **RS-1**. Herein we report the fluorescent sensing properties of the PET/AIE-based fluorescent sensor EN-1 for the detection of water in a low water content region and from moderate to high water content regions in THF, which are suitable for a large-scale industrial process as well as quality inspection of products.

## Results and discussion

The PET/AIE-based fluorescent sensor **EN-1** was synthesized according to a stepwise synthetic protocol (Scheme 1). The starting compound **TPE-(An-CHO)$_4$** composed of a TPE core and four anthraldehydes as peripheral units has been reported elsewhere.[45] **TPE-(An-CHO)$_4$** was treated with a solution of methylamine to give the intermediate imine, which was then reduced with sodium borohydride to give **TPE-(An-NMe)$_4$**. The reaction of **TPE-(An-NMe)$_4$** with 3-(bromomethyl)-4-(4,4,5,5-tetramethyl-1,3,2-dioxaborolan-2-yl)benzonitrile yielded **EN-1**. The characterization of **EN-1** was successfully determined by FTIR, $^1$H and $^{13}$C NMR measurements, and HRMS analysis.

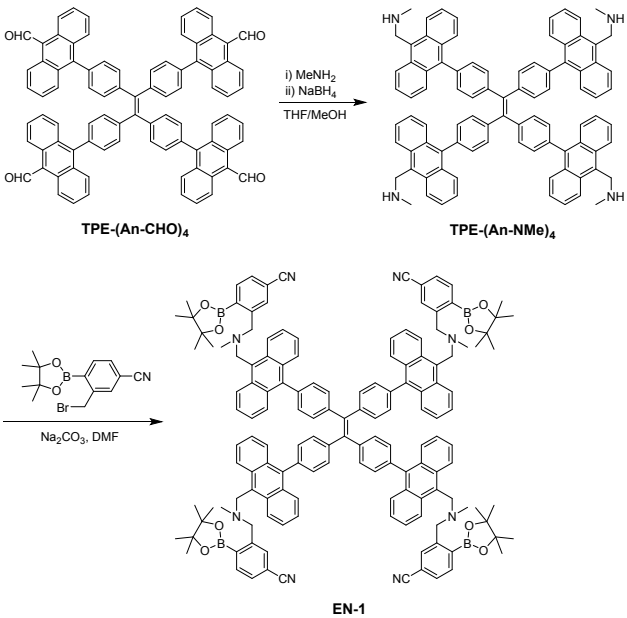


**Scheme 1** Synthesis of **EN-1**.

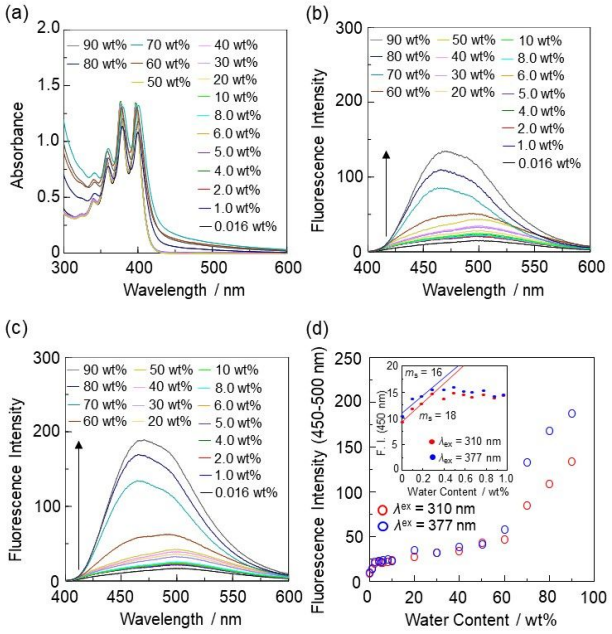


**Fig. 2** (a) Photoabsorption spectra of **EN-1** ($c$ = 2.0 × 10$^{-5}$ M) in THF containing water (0.016–90 wt%). Fluorescence spectra of **EN-1** ($c$ = 2.0 × 10$^{-5}$ M) by $\lambda^{ex}$ at (b) 310 nm and (c) 377 nm in THF containing water (0.016–90 wt%). (d) Fluorescence peak intensity at 450–500 nm of **EN-1** by $\lambda^{ex}$ at 310 nm and 377 nm as a function of water content (0.016–90 wt%) in THF; the inset in (d) is fluorescence peak intensity at 450 nm of **EN-1** by $\lambda^{ex}$ at 310 nm and 377 nm as a function of water content below 1.0 wt% in THF.

Photoabsorption and fluorescence spectra of **EN-1** were measured in THF containing various concentrations of water (Fig. 2a–c). In absolute THF (with 0.016 wt% water content), **EN-1** showed a photoabsorption band in the range from 300 to 350 nm and a vibronic-structured photoabsorption band in the range from 350 to 400 nm, which were assigned to the TPE core and the anthracene skeleton, respectively (Fig. 2a). In the water content region below 50 wt%, the photoabsorption spectra of **EN-1** showed unnoticeable changes with the increase in the water content in the THF solutions. On the other hand, level-off photoabsorption spectral tails in the long wavelength region were observed in the water content region greater than 60 wt%, indicating the presence of nanosized or micrometer-sized particles. The fluorescence spectra of **EN-1** in THF were obtained by photoexcitation ($\lambda^{ex}$) at 310 nm and 377 nm corresponding to the TPE core at 300–350 nm (Fig. 2b) and the anthracene skeleton at 350–400 nm, respectively (Fig. 2c). By $\lambda^{ex}$ at both 310 nm and 377 nm, **EN-1** in absolute THF exhibited a bimodal and broad fluorescence band in the range of 400 nm to 600 nm with fluorescence maximum wavelengths ($\lambda_{max}^{fl}$) at ca. 450 nm and ca. 500 nm originating from the anthracene skeleton and the TPE core, respectively. However, the fluorescence properties of **EN-1** in absolute THF were almost quenched, as with the case of **OF-2** and **RS-1**.[37,75] This is attributed to the fact that the PET takes place from the amino moiety to the photoexcited anthracene skeleton and the dynamic rotation of the phenyl groups of the TPE core is active in the

absence of water. Upon the addition of water to the THF solution of **EN-1**, the bimodal fluorescence band increased in the intensity with the increase in the water content until 90 w%. In the low water content region below 1.0 wt%, an enhancement of the fluorescence band at around 450 nm originating from the anthracene skeleton as well as that at around 500 nm was observed (see Fig. S6 for photoabsorption and fluorescence spectra in the low water content region below 1.0 wt%, ESI†), which is attributed to the formation of the PET inactive (fluorescent) species **EN-1($H_2O$)** by the addition of water molecules (Fig. 1c). With increasing the water content from 10 wt% to 50 wt%, the fluorescence intensity at around 500 nm originating from the TPE core gradually increased, which is attributed to the RIR of TPE[69–71] due to the increase in viscosity of the THF-water mixtures,[76] although such increase in the fluorescence intensity in the moderate water content region was not observed in the case of **RS-1**.[75] Furthermore, a significant enhancement of the fluorescence band at around 470 nm was observed in the high water content region above 60 wt%, which is due to the AIE characteristics associated with aggregate formation of **EN-1($H_2O$)-A** in both PET inactive and RIR states. It is worth mentioning here that the AIE characteristics of **EN-1** were observed from the relatively low water content of 60 wt% compared with **RS-1**, which exhibited the AIE characteristics in the high water content region over 75 wt%.

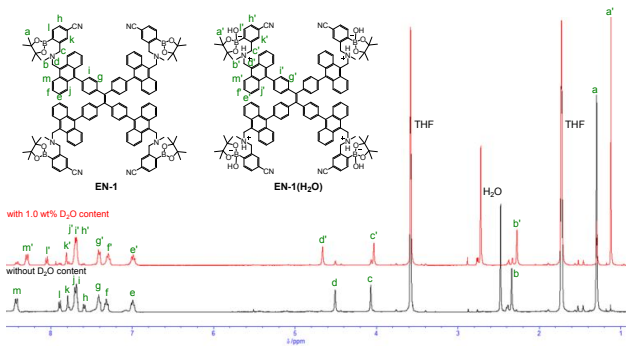


**Fig. 3** $^1$H NMR spectra of **EN-1** ($2.0 \times 10^{-2}$ M) in THF-$d_8$ without $D_2O$ and with 1.0 wt% $D_2O$ content.

To confirm the formation of the PET inactive species **EN-1($H_2O$)** by the addition of water molecules, we performed $^1$H NMR spectral measurements on **EN-1** with and without the addition of deuterated water ($D_2O$) in the THF-$d_8$ solution ($2.0 \times 10^{-2}$ M) (Fig. 3). The $^1$H NMR spectrum of **EN-1** in THF-$d_8$ without the addition of $D_2O$ shows obvious signals assigned to a single chemical species, **EN-1**. The $^1$H NMR spectrum of **EN-1** in THF-$d_8$ with $D_2O$ content of 1.0 wt% can be assigned to another single chemical species different from **EN-1**. Upon the addition of 1.0 wt% $D_2O$ to the THF-$d_8$ solution of **EN-1**, the signals of the methyl protons $H_a$ of boronic acid pinacol ester and the aromatic protons $H_m$ of the anthracene skeleton showed considerable upfield shifts, but those of the aromatic protons $H_h$ and $H_l$ of the cyanophenyl groups and the methylene protons $H_d$ next to the anthracene skeleton showed considerable downfield shifts. Consequently, the fact strongly indicates that the PET inactive species **EN-1($H_2O$)** interacted with water molecules occurred upon the addition of water to the **EN-1** solution (see Fig. S5 for $^1$H NMR spectra with $H_2O$).

The aggregate formation of **EN-1** in THF with 60–90 wt% water content was determined by Tyndall scattering (Fig. 4a). In addition, to demonstrably confirm the formation of aggregates, we performed scanning electron microscopy (SEM) for the substances that were obtained from the THF solutions of **EN-1** with 60 wt%, 70 wt%, and 90 wt% water content (Fig. 4b). The SEM image for **EN-1** in THF with 60 wt% water content displayed the formation of particle aggregates with an average size of 600 nm, which caused the appearance of the level-off photoabsorption spectral tails and the increase in the fluorescence intensity at around 470 nm (Fig. 2). On the other hand, the formation of particle aggregates with average sizes of 50–150 nm was also confirmed in the SEM images for **EN-1** in THF with 70 wt% and 90 wt% water content, which drastically enhanced the fluorescence emission. A decrease in particle size with an increase in water content is commonly observed in the AIE mechanism, indicating that the smaller particle aggregates resulted in the increase in the fluorescence intensity.[43,52,58,77,78] Consequently, the SEM measurements as well as Tyndall scattering demonstrated the aggregate formation of **EN-1($H_2O$)-A** in both PET inactive and RIR states, leading to the significant enhancement of the fluorescence band at around 470 nm in the water content region above 60 wt% in the THF solution.

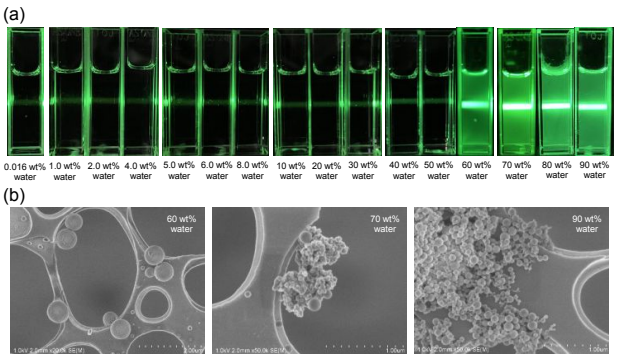


**Fig. 4** (a) Tyndall scattering of **EN-1** in absolute THF (0.016 wt% water) and THF with 1.0–90 wt% water content under irradiation with a laser beam. (b) SEM images of substances obtained from THF solutions of **EN-1** with 60 wt%, 70 wt%, and 90 wt% water content.

Furthermore, to confirm the fluorescence properties of **EN-1** originating from the anthracene skeleton and the TPE core, the photoabsorption and fluorescence spectral measurements of **EN-1** were performed in 2-methylthetrahydrofuran (2-MeTHF) at room temperature (298 K) and the glassy matrix of 2-MeTHF at 77 K, in which the dynamic rotation of the TPE core was restricted (Fig. 5). The photoabsorption spectrum of **EN-1** in the glassy matrix at 77 K was similar to that in 2-MeTHF at 298 K (Fig. 5a); at both 77 K and 298 K, **EN-1** exhibited the photoabsorption band at 300–350 nm originating from the TPE core and the vibronic-structured photoabsorption band at 350–400 nm originating from the anthracene skeleton. The

fluorescence spectrum of **EN-1** in 2-MeTHF at 298K exhibited a broad fluorescence band in the range of 400 nm to 600 nm with a $\lambda_{max}^{fl}$ at ca. 500 nm originating from the TPE core and a shoulder fluorescence band at around 450 nm originating from the anthracene skeleton, although the fluorescence properties were almost quenched as with the case of the THF solution at 298 K (Fig. 2b, c). On the other hand, **EN-1** in the glassy matrix at 77 K showed a relatively narrow fluorescence band with a $\lambda_{max}^{fl}$ at ca. 450 nm originating from the anthracene skeleton and a shoulder band at around 475 nm, which is associated with the fluorescence band at 470 nm due to the aggregate formation observed in the THF solution with the water content above 60 wt% (Fig. 2b–d). Additionally, we measured the solid-state UV-Vis diffuse reflection–absorption and fluorescence spectra for the solid of **EN-1** (Fig. 5b). The photoabsorption band of **EN-1** in the solid state appeared at 350–450 nm, which was similar to that in the aggregate state formed in the THF solution with the water content above 60 wt% (Fig. 2a), although the photoabsorption band in the solid state was broadened compared with that in the aggregate state. The corresponding fluorescence spectrum of **EN-1** in the solid state showed a broad fluorescence band in the range of 400 nm to 600 nm with a $\lambda_{max}^{fl}$ at ca. 485 nm, which was similar to the fluorescence band ($\lambda_{max}^{fl}$ = ca. 470 nm) of **EN-1** in the aggregate state (Fig. 2b, c). Therefore, these facts indicate that the fluorescence properties of **EN-1** in both the aggregate state and the solid state were not derived from anthracene dimer or excimer emission[17,18] but were due to the AIE characteristics associated with the aggregate formation of **EN-1($H_2O$)-A** in both PET inactive and RIR states (Fig. 1c).

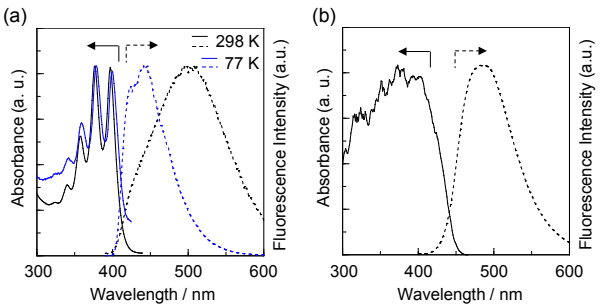


**Fig. 5** (a) Photoabsorption and fluorescence spectra ($\lambda^{ex}$ = 377 nm) of **EN-1** ($c$ = 2.0 × $10^{-5}$ M) in 2-MeTHF at 298 K and the glassy matrix of 2-MeTHF at 77K. (b) UV-Vis diffuse reflection–absorption and fluorescence spectra ($\lambda^{ex}$ = 377 nm) of **EN-1** in the solid state.

Finally, to clarify the PET, RIR, and AIE processes of **EN-1** with the increase in the water content in the solution, the fluorescence intensity at 450–500 nm by $\lambda^{ex}$ at 310 nm or 377 nm were plotted against the water fraction in the THF solution (Fig. 2d). By $\lambda^{ex}$ at both 310 nm and 377 nm, the fluorescence intensity increased almost linearly with the increase in the water content until 0.4 wt% due to the suppression of PET (Fig. 2d inset). Thus, the slope ($m_s$) values for the enhancement of the fluorescence intensity were determined from the calibration curves (the linear least squares method) for the plots of the fluorescence peak intensity *versus* the water fraction in the low water content region below 0.3 wt%. The $m_s$ values of **EN-1** in THF were 18 and 16 in $\lambda^{ex}$ at 310 nm and 377 nm, respectively. The correlation coefficient ($R^2$) values of the calibration curves were ca. 0.9, indicating the relatively good linearity. It is worth mentioning here that the $m_s$ values of **EN-1** in THF were much smaller than those (390) of **OF-2** but larger than those (5.8–6.7) of **RS-1**. Thus, the DL of **EN-1** was determined from the plot of the fluorescence intensity at ca. 450 nm ($\lambda^{ex}$ = 377 nm) as a function of the water content in the THF solution in the water content region below 0.3 wt% (Fig. 2d inset; DL = 3.3$\sigma/m_s$, where $\sigma$ is the standard deviation of the blank sample and $m_s$ is the slope of the calibration curve). The DL of **ET-1** for water in THF was 0.21 wt%, which was inferior to that (0.008 wt%) of **OF-2**[37] but superior to that (0.49 wt%) of **RS-1**.[75] Compared with **OF-2**, the deterioration of the DL value of **EN-1** is attributed to the dynamic rotation of the TPE unit, which is directly attached to the anthracene skeleton, leading to the non-radiative decay of the photoexcited anthracene skeleton. Compared with **RS-1**, on the other hand, the improvement of the DL value of **EN-1** is ascribable to the fact that the four anthracene-AminoMeCNPhenylBPin units led to the increased fluorescence emission originating from the anthracene skeleton. In the moderate water content range of 10–50 wt%, the fluorescence intensity at around 500 nm originating from the TPE core by the RIR gradually increased with the increase in the water content, that is, viscosity of the THF-water mixtures. Moreover, the plots reveal that in the high water content region above 60 wt%, the fluorescence intensity at around 470 nm corresponding to the AIE characteristics increased dramatically and almost linearly with the increase in the water content. Indeed, the linear relationship in the AIE characteristics in the THF solution was clearly demonstrated in the calibration curves for the plots of the fluorescence peak intensity *versus* the water fraction over 50 wt%; the $m_s$ and $R^2$ values were 2.4 and 0.96 in $\lambda^{ex}$ at 310 nm and 4.0 and 0.95 in $\lambda^{ex}$ at 377 nm, respectively. The AIE characteristics of **EN-1** in the relatively low water content region is ascribable to the fact that the four anthracene-AminoMeCNPhenylBPin units lowered its solubility in solvent-water mixtures, compared with **RS-1** having an AminoMeCNPhenylBPin unit. Consequently, this work reveals that **EN-1** composed of a TPE core and four anthracene-AminoMeCNPhenylBPin units can act as a PET/AIE-based fluorescent sensor for the detection of water in the low water content region and from the moderate to high water content regions in solvents, although the DL of the PET/AIE-based fluorescent sensor for water is still inferior to that of the PET-based fluorescent sensor for water.[37]

## Conclusions

We have designed and developed **EN-1** composed of a tetraphenylethen (TPE) core and four anthracene-(aminomethyl)-4-cyanophenylboronic acid pinacol esters (AminoMeCNPhenylBPin) as peripheral units as a PET (photo-induced electron transfer)/AIE (aggregation-induced emission)-based fluorescent sensor for water over a wide range from low to

high water content regions in solvents. It was found that in the low water content region below 1.0 wt%, the enhancement of the fluorescence band originating from the anthracene skeleton with the increase in the water content is attributed to the formation of the PET inactive (fluorescent) species **EN-1($H_2O$)** by the addition of water molecules. In the moderate water content region from 10 wt% to 50 wt%, the fluorescence intensity originating from the TPE core gradually increased with the increase in the water content, which can be ascribed to the restricted intramolecular rotation (RIR) of TPE due to the increase in viscosity of the THF-water mixtures. Furthermore, in the high water content region above 60 wt%, the significant enhancement of the fluorescence band with the increase in the water content was due to the AIE characteristics associated with the aggregate formation of **EN-1($H_2O$)-A** in both PET inactive and RIR states. Compared with a PET/AIE-based fluorescent sensor composed of a TPE unit and an AminoMeCNPhenylBPin unit, the improvement of the detection limit (DL) value for water and AIE characteristics of **EN-1** in the relatively low water content region is ascribable to the fact that the four anthracene-AminoMeCNPhenylBPin units led to the increased fluorescence emission originating from the anthracene skeleton and its low solubility in solvent-water mixtures. Consequently, this work demonstrates that **EN-1** composed of a TPE core and four anthracene-AminoMeCNPhenylBPin units can act as a PET/AIE-based fluorescent sensor for the detection of water in the low water content region and from the moderate to high water content regions in solvents.

## Experimental

### General

Melting points were measured with AS ONE ATM-02. IR spectra were recorded on a SHIMADZU IRTracer-100 spectrometer by the ATR method. $^1$H and $^{13}$C NMR spectra were recorded on a Varian-400 FT NMR spectrometer. High-resolution mass spectral data GC-FD were acquired on a JEOL JMS-T100 GCV 4G. Recycling gel permeation chromatography (GPC) was performed using an RI-detector (GL Science RI 704), a pomp (GILSON 307 PUMP), and two columns (Shodex GPC H-2001L). Photoabsorption spectra were observed with a SHIMADZU UV-3600 plus spectrophotometer. Fluorescence spectra of **EN-1** in THF were measured with a Hitachi F-4500 spectrophotometer. Fluorescence spectra of **EN-1** in 2Me-THF were measured with a HORIBA FluoroMax-4 spectrophotometer. The addition of water to THF solutions containing **EN-1** was made in terms of weight percent (wt%). The determination of water in THF was done with an MKC-610 and MKA-610 Karl Fischer moisture titrator (Kyoto Electronics Manufacturing Co., Ltd) based on Karl Fischer coulometric titration for below 1.0 wt% and volumetric titration for 1.0–90 wt%. The solid morphology was observed using a Hitachi S-4800 scanning electron microscope (SEM) coupled with an energy dispersive X-ray (EDX) analyzer. The dispersed samples in solution were dried on a carbon-coated copper grid without any metal coating.

### Synthesis

**1,1',1'',1'''-((Ethene-1,1,2,2-tetrayltetrakis(benzene-4,1-diyl))tetrakis(anthracene-10,9-diyl))tetrakis(*N*-methylmethanamine) (TPE-(An-NMe)$_4$):** A solution of **TPE-(An-CHO)$_4$** (0.1 g, 0.087 mmol) and methylamine (14 mL, 28 mmol) in THF (120 mL)/methanol (40 mL) was stirred for 24 h at room temperature under an nitrogen atmosphere. The reaction mixture was cooled to 0 °C. Next, sodium borohydride (0.70 g, 18.5 mmol) was added to the reaction mixture, and the reaction mixture was stirred at 0 °C for 0.5 h. The reaction mixture was concentrated to be 100 mL, and then, dichloromethane was added to the reaction mixture. The solution was filtered and concentrated. The resulting residue was dissolved in dichloromethane and subjected to reprecipitation by *n*-hexane to afford **TPE-(An-NMe)$_4$** (0.05 g, yield 50 %) as a light-yellow solid; 270 °C (decomposition); FT-IR (ATR): = 3065, 2841, 2783, 1510 , 1468, 1443, 1387, 1341, 1103 cm$^{-1}$; $^1$H NMR (400 MHz, $CDCl_3$): $\delta$ = 1.68 (br, NH), 2.75 (s, 12H), 4.78 (s, 8H), 7.06–7.10 (m, 8H), 7.39–7.45 (m, 16H), 7.64–7.67 (m, 8H), 7.72–7.76 (m, 8H), 8.40 (d, $J$ = 9.0 Hz, 8H) ppm; $^{13}$C NMR (100 MHz, $CDCl_3$): $\delta$ = 22.08, 37.35, 124.08, 125.28, 126.03, 127.82, 130.08, 130.18, 130.86, 130.94, 131.82, 137.52, 137.89, 142.16, 142.98 ppm; HRMS (GC-FD): *m*/*z* (%): [M$^{+\bullet}$] calcd. for $C_{90}H_{72}N_4$, 1208.57570; found 1208.57577.

**3,3',3'',3'''-(((((Ethene-1,1,2,2-tetrayltetrakis(benzene-4,1-diyl))tetrakis(anthracene-10,9-diyl))tetrakis(methylene))tetrakis(methylazanediyl))tetrakis(methylene))tetrakis(4-(4,4,5,5-tetramethyl-1,3,2-dioxaborolan-2-yl)benzonitrile) EN-1:** To a DMF solution (40 mL) of **TPE-(An-NMe)$_4$** (0.04 g, 0.033 mmol) and $Na_2CO_3$ (0.056 g, 0.53 mmol) at room temperature under an argon atmosphere added a DMF solution (10 mL) of 3-(bromomethyl)-4-(4,4,5,5-tetramethyl-1,3,2-dioxaborolan-2-yl)benzonitrile (0.053 g, 0.17 mmol). After stirring for 24 h, the reaction mixture was filtered and concentrated. The resulting residue was dissolved in dichloromethane. The dichloromethane solution was filtered and concentrated. Recycling GPC (chloroform as eluent) for the residue was performed to give **EN-1** (0.03 g, yield 40%) as a light-yellow solid; 270 °C (decomposition); FT-IR (ATR): = 2976, 2230, 1605, 1549, 1495, 1445, 1400, 1344, 1271, 1213, 1142, 1063 cm$^{-1}$; $^1$H NMR (400 MHz, $CD_2Cl_2$): $\delta$ = 1.31 (s, 48H), 2.35 (s, 12H), 4.01 (s, 8H), 4.53 (s, 8H), 7.03–7.09 (m, 8H), 7.39–7.44 (m, 16H), 7.52 (d, $J$ = 8.0 Hz, 4H), 7.69–7.73 (m, 20H), 7.83 (d, $J$ = 7.6 Hz, 4H), 8.41 (d, $J$ = 8.8 Hz, 8H) ppm; $^{13}$C NMR (100 MHz, $CD_2Cl_2$): $\delta$ = 25.16, 43.00, 53.04, 61.08, 84.46, 113.91, 119.42, 125.28, 125.39, 125.46, 125.68, 127.78, 129.87, 130.14, 130.25, 131.17, 131.41, 132.08, 132.42, 135.77, 138.08, 138.15, 142.34, 143.38, 147.06 ppm; HRMS (GC-FD): *m*/*z* (%): [M$^{+\bullet}$] calcd. for $C_{146}H_{136}B_4N_8O_8$, 2173.08533; found 2173.08977.

## Conflicts of interest

There are no conflicts to declare.

## Acknowledgements

This work was supported by Grants-in-Aid for Scientific Research (B) from the Japan Society for the Promotion of Science (JSPS) KAKENHI Grant Number 19H02754 and 22H02123, JST Adaptable and Seamless Technology transfer Program through Target-driven R&D (A-STEP) Grant Number JPMJTM20RB, and by Nakanishi Scholarship Foundation.

## Notes and references

1 S. Mishra and A. K. Singh, *Coord. Chem. Rev.*, 2021, **445**, 214063.
2 W. Cheng, Y. Xie, Z. Yang, Y. Sun, M.-Z. Zhang, Y. Ding and W. Zhang, *Anal. Chem.*, 2019, **91**, 5817–5823.
3 J. Othong, J. Boonmak, F. Kielar and S. Youngme, *ACS Appl. Mater. Interfaces*, 2020, **12**, 41776–41784.
4 Y. Zhou, G. Baryshnikov, X. Li, M. Zhu, H. Ågren and L. Zhu, *Chem. Mater.*, 2018, **30**, 8008–8016.
5 F. Wu, L. Wang, H. Tang and D. Cao, *Anal. Chem.*, 2019, **91**, 5261–5269.
6 H. S. Jung, P. Verwilst, W. Y. Kim and J. S. Kim, *Chem. Soc. Rev.*, 2016, **45**, 1242–1256.
7 P. Kumar, R. Sakla, A. Ghosh and D. A. Jose, *ACS Appl. Mater. Interfaces*, 2017, **9**, 25600–25605.
8 S. Song, Y. Zhang, Y. Yang, C. Wang, Y. Zhou, C. Zhang, Y. Zhao, M. Yang and Q. Lin, *Analyst*, 2018, **143**, 3068–3074.
9 H. Yan, S. Guo, F. Wu, P. Yu, H. Liu, Y. Li and L. Mao, *Angew. Chem. Int. Ed.*, 2018, **57**, 3922–3926.
10 T. Maeda and F. Würthner, *Chem. Commun.*, 2015, **51**, 7661–7664.
11 P. Kumar, A. Ghosh and D. A. Jose, *ChemistrySelect*, 2021, **6**, 820–842.
12 L. Liu, Q. Zhang, H. Duan, C. Li and Y. Lu, *Anal. Methods*, 2021, **13**, 3792–3798.
13 S. Roy, S. Das, A. Ray and P. P. Parui, *New J. Chem.*, 2021, **45**, 4574–4583.
14 W.-E. Lee, Y.-J. Jin, L.-S. Park and G. Kwak, *Adv. Mater.*, 2012, **24**, 5604–5609.
15 D.-C. Han, Y.-J. Jin, J.-H. Lee, S.-I. Kim, H.-J. Kim, K.-H. Song and G. Kwak, *Macromol. Chem. Phys.*, 2014, **215**, 1068–1076.
16 J. Lee, M. Pyo, S. Lee, J. Kim, M. Ra, W.-Y. Kim, B. J. Park, C. W. Lee and J.-M. Kim, *Nat. Commun.*, 2014, **5**, 3736.
17 T. Fumoto, S. Miho, Y. Mise, K. Imato and Y. Ooyama, *RSC Adv.,* 2021, **11**, 17046–17050.
18 S. Miho, T. Fumoto, Y. Mise, K. Imato, S. Akiyama, M. Ishida and Y. Ooyama, *Mater. Adv.,* 2021, **2**, 7662–7670.
19 D. Citterio, K. Minamihashi, Y. Kuniyoshi, H. Hisamoto, S. Sasaki and K. Suzuki, *Anal. Chem.*, 2001, **73**, 5339–5345.
20 C.-G. Niu, A.-L. Guan, G.-M. Zeng, Y.-G. Liu and Z.-W. Li, *Anal. Chim. Acta*, 2006, **577**, 264–270.
21 Z.-Z. Li, C.-G. Niu, G.-M. Zeng and P.-Z. Qin, *Chem. Lett.*, 2009, **38**, 698–699.
22 C.-G. Niu, P.-Z. Qin, G.-M. Zeng, X.-Q. Gui and A.-L. Guan, *Anal. Bioanal. Chem.*, 2007, **387**, 1067–1074.
23 Z. Li, Q. Yang, R. Chang, G. Ma, M. Chen and W. Zhang, *Dyes Pigm.*, 2011, **88**, 307–314.
24 W. Chen, Z. Zhang, X. Li, H. Ågren and J. Su, *RSC Adv.*, 2015, **5**, 12191–12201.
25 S. Tsumura, T. Enoki and Y. Ooyama, *Chem. Commun.*, 2018, **54**, 10144–10147.
26 T. Enoki and Y. Ooyama, *Dalton Trans.*, 2019, **48**, 2086–2092.
27 K. Imato, T. Enoki and Y. Ooyama, *RSC Adv.*, 2019, **9**, 31466–31473.
28 S. Tusmura, K. Ohira, K. Imato and Y. Ooyama, *RSC Adv.*, 2020, **10**, 33836–33843.
29 I. M. Resta and F. Galindo, *Dyes Pigm.*, 2022, **197**, 109908.
30 W. Liu, Y. Wang, W. Jin, G. Shen and R. Yu, *Anal. Chim. Acta*, 1999, **383**, 299–307.
31 J. S. Kim, M. G. Choi, Y. Huh, M. H. Kim, S. H. Kim, S. Y. Wang and S.-K. Chang, *Bull. Korean Chem. Soc.*, 2006, **27**, 2058–2060.
32 H. Mishra, V. Misra, M. S. Mehata, T. C. Pant and H. B. Tripathi, *J. Phys. Chem. A*, 2004, **108**, 2346–2352.
33 A. C. Kumar and A. K. Mishra, *Talanta*, 2007, **71**, 2003–2006.
34 Y. Ooyama, M. Sumomogi, T. Nagano, K. Kushimoto, K. Komaguchi, I. Imae and Y. Harima, *Org. Biomol. Chem.*, 2011, **9**, 1314–1316.
35 Y. Ooyama, A. Matsugasako, K. Oka, T. Nagano, M. Sumomogi, K. Komaguchi, I. Imae and Y. Harima, *Chem. Commun.*, 2011, **47**, 4448–4450.
36 Y. Ooyama, A. Matsugasako, Y. Hagiwara, J. Ohshita and Y. Harima, *RSC Adv.*, 2012, **2**, 7666–7668.
37 Y. Ooyama, K. Furue, K. Uenaka and J. Ohshita, *RSC Adv.*, 2014, **4**, 25330–25333.
38 Y. Ooyama, M. Hato, T. Enoki, S. Aoyama, K. Furue, N. Tsunoji and J. Ohshita, *New J. Chem.*, 2016, **40**, 7278–7281.
39 Y. Ooyama, R. Nomura, T. Enoki, R. Sagisaka, N. Tsunoji and J. Ohshita, *ChemistrySelect*, 2017, **2**, 7765–7770.
40 D. Jinbo, K. Imato and Y. Ooyama, *RSC Adv.*, 2019, **9**, 15335–15340.
41 D. Jinbo, K. Ohira, K. Imato and Y. Ooyama, *Mater. Adv.,* 2020, **1**, 354–362.
42 F. Khan, A. Ekbote, S. M. Mobin and R. Misra, *J. Org. Chem.*, 2021, **86**, 1560–1574.
43 X. Y. Shen, Y. J. Wang, H. Zhang, A. Qin, J. Z. Sun and B. Z. Tang, *Chem. Commun.*, 2014, **50**, 8747–8750.
44 L. Ding, Z. Zhang, X. Li and J. Su, *Chem. Commun.*, 2013, **49**, 7319–7321.
45 Y. Mise, K. Imato, T. Ogi, N. Tsunoji and Y. Ooyama, *New J. Chem.,* 2021, **45**, 4164–4173.
46 Y. Zhang, D. Li, Y. Li and J. Yu, *Chem. Sci.*, 2014, **5**, 2710–2716.
47 N. Zhao, Z. Yang, J. W. Y. Lam, H. H. Y. Sung, N. Xie, S. Chen, H. Su, M. Gao, I. D. Williams, K. S. Wong and B. Z. Tang, *Chem. Commun.,* 2012, **48**, 8637–8639.
48 J. Luo, Z. Xie, J. W. Y. Lam, L. Cheng, H. Chen, C. Qiu, H. S. Kwok, X. Zhan, Y. Liu, D. Zhu and B. Z. Tang, *Chem. Commun.*, 2001, 1740–1741.
49 J. Wang, B. Yue, X. Jia, R. Cao, X. Niu, H. Zhao, J. Li and L. Zhu, *Chem. Commun.*, 2022, doi.org/10.1039/D1CC06931D.
50 Y. Chen, B. Wang, Y. Lei, Y. Zhou, Y. Guo, M. Liu, W. Gao, X. Huang and H. Wu, *Mater. Chem. Front.*, 2022, **6**, 459–465.
51 R. Ding, K. Qin, H. Sun, S. Zhou, S. Guo, H. Feng, H. Ma and Z. Qian, *J. Mater. Chem. C*, 2021, **9**, 12177–12183.
52 Y. Hong, J. W. Y. Lama and B. Z. Tang, *Chem. Commun.*, 2009, 4332–4353.
53 J. Mei, N. L. C. Leung, R. T. K. Kwok, J. W. Y. Lam and B. Z. Tang, *Chem. Rev.*, 2015, **115**, 11718–11940.
54 Q. Yan and S. Wang, *Mater. Chem. Front.*, 2020, **4**, 3153–3175.
55 J. Li, J. Wang, H. Li, N. Song, D. Wang and B. Z. Tang, *Chem. Soc. Rev.,* 2020, **49**, 1144–1172.
56 Y. Zhang, D. Li, Y. Li and J. Yu, *Chem. Sci.*, 2014, **5**, 2710–2716.
57 J. Tong, Y. Wang, J. Mei, J. Wang, A. Qin, J. Z. Sun and B. Z. Tang, *Chem. Eur. J.*, 2014, **20**, 4661–4670.

58 X. Y. Shen, Y. J. Wang, E. Zhao, W. Z. Yuan, Y. Liu, P. Lu, A. Qin, Y. Ma, J. Z. Sun and B. Z. Tang, *J. Phys. Chem. C*, 2013, 117, **14**, 7334–7347.
59 N. Zhao, Z. Yang, J. W. Y. Lam, H. H. Y. Sung, N. Xie, S. Chen, H. Su, M. Gao, I. D. Williams, K. S. Wong and B. Z. Tang, *Chem. Commun.,* 2012, **48**, 8637–8639.
60 F. Khan, A. Ekbote, S. M. Mobin and R. Misra, *J. Org. Chem*., 2021, **86**, 1560–1574.
61 W. Guan, W. Zhou, C. Lu and B. Z. Tang, *Angew. Chem. Int. Ed*., 2015, **54**, 15160–15164.
62 J.-B. Xiong, H.-T. Feng, J.-P. Sun, W.-Z. Xie, D. Yang, M. Liu and Y.-S. Zheng, *J. Am. Chem. Soc*., 2016, **138**, 11469–11472.
63 Q.-Y. Li, Z. Ma, W.-Q. Zhang, J.-L. Xu, W. Wei, H. Lu, X. Zhao and X.-J. Wang, *Chem. Commun.,* 2016, **52**, 11284–11287.
64 X. Liu and G. Liang, *Chem. Commun.,* 2017, **53**, 1037–1040.
65 C. Gui, E. Zhao, R. T. K. Kwok, A. C. S. Leung, J. W. Y. Lam, M. Jiang, H. Deng, Y. Cai, W. Zhang, H. Su and B. Z. Tang, *Chem. Sci*., 2017, **8**, 1822–1830.
66 Y. Ooyama, M. Sugino, T. Enoki, K. Yamamoto, N. Tsunoji and J. Ohshita, *New J. Chem.*, 2017, **47**, 4747–4749.
67 A. Thakuri, M. Banerjee and A. Chatterjee, *ChemPhotoChem*, 2022, doi.org/10.1002/cptc.202100234.
68 C. Gao, J. Y. Seow, B. Zhang, C. R. Hall, A. J. Tilley, J. M. White, T. A. Smith and W. W. H. Wong, *ChemPlusChem*, 2019, **84**, 746–753.
69 Y. Dong, J. W. Y. Lam, A. Qin, J. Liu, Z. Li and B. Z. Tang, *Appl. Phys. Chem.*, 2007, **91**, 011111.
70 H. Zhang, Y. Nie, J. Miao, D. Zhang, Y. Li, G. Liu, G. Sun and X. Jiang, *J. Mater. Chem. C*, 2019, **7**, 3306–3314.
71 X. Li, Y. Yin, H. Yan and C. Lu, *Chem. Asian J*., 2017, **12**, 2207–2210.
72 K. Nishino, H. Yamamoto, J. Ochi, K. Tanaka and Y. Chujo, *Chem. Asian J*., 2019, **14**, 1577–1581.
73 K. Tanaka, K. Nishino, S. Ito, H. Yamane, K. Suenaga, K. Hashimoto and Y. Chujo, *Faraday Discuss*., 2017, **196**, 31–42.
74 H. Mori, K. Nishino, K. Wada, Y. Morisaki, K. Tanaka and Y. Chujo, *Mater. Chem. Front*., 2018, **2**, 573–579.
75 Y. Ooyama, R. Sagisaka, T. Enoki, N. Tsunoji and J. Ohshita, *New J. Chem*., 2018, **42**, 13339–13350.
76 J. Hao, H. Cheng, P. Butler, L. Zhang and C. C. Han, *J. Chem. Phys*., 2010, **132**, 154902.
77 S. Odabas, E. Tekin, F. Turksoy and C. Tanyeli, *J. Mater. Chem. C*, 2013, **1**, 7081–7091.
78 H. Zhou, J. Li, M. H. Chua, H. Yan, Q. Ye, J. Song, T. T. Lin, B. Z. Tang and J. Xu, *Chem. Commun.,* 2016, **52**, 12478–12481.